

Current Biology

Localization of stomatal lineage proteins reveals contrasting planar polarity patterns in *Arabidopsis* cotyledons

Highlights

- Cotyledons exhibit two polarity patterns: mediolateral and proximodistal
- We find no evidence that cell polarity is influenced by mechanical stretching
- Cell polarity is less coordinated in stomatal compared with non-stomatal lineages

Authors

John A. Fozard, Man Yu, William Bezodis, ..., Catherine Mansfield, Jordi Chan, Enrico Coen

Correspondence

jordi.chan@jic.ac.uk (J.C.),
enrico.coen@jic.ac.uk (E.C.)

In brief

Fozard, Yu, Bezodis et al. reveal that cellular localization of stomatal polarity proteins is biased in cotyledons toward medial positions in stomatal lineages and toward proximal positions in non-stomatal lineages. They find no evidence that mechanical stretching reorients polarity, in contrast to a previous report.

Report

Localization of stomatal lineage proteins reveals contrasting planar polarity patterns in *Arabidopsis* cotyledons

John A. Fozard,^{1,4} Man Yu,^{1,4} William Bezodis,^{1,4} Jie Cheng,^{1,2,3} Jamie Spooner,¹ Catherine Mansfield,¹ Jordi Chan,^{1,*} and Enrico Coen^{1,5,6,*}

¹Department of Cell and Developmental Biology, John Innes Centre, Norwich NR4 7UH, UK

²Present address: State Key Laboratory of Systematic and Evolutionary Botany, CAS Center for Excellence in Molecular Plant Sciences, Institute of Botany, Chinese Academy of Sciences, Beijing 100093, China

³Present address: College of Life Sciences, University of Chinese Academy of Sciences, Beijing 100049, China

⁴These authors contributed equally

⁵Twitter: @InnerWorlds1

⁶Lead contact

*Correspondence: jordi.chan@jic.ac.uk (J. C.), enrico.coen@jic.ac.uk (E. C.)

<https://doi.org/10.1016/j.cub.2022.09.049>

SUMMARY

Many plant cells exhibit polarity, revealed by asymmetric localization of specific proteins within each cell.^{1–6} Polarity is typically coordinated between cells across a tissue, raising the question of how coordination is achieved. One hypothesis is that mechanical stresses provide cues.⁷ This idea gains support from experiments in which cotyledons were mechanically stretched transversely to their midline.⁸ These previously published results showed that without applied tension, the stomatal lineage cell polarity marker, BREVIS RADIX-LIKE 2 (BRXL2), exhibited no significant excess in the transverse orientation. By contrast, 7 h after stretching, BRXL2 polarity distribution exhibited transverse excess, aligned with the stretch direction. These stretching experiments involved statistical comparisons between snapshots of stretched and unstretched cotyledons, with different specimens being imaged in each case.⁸ Here, we image the same cotyledon before and after stretching and find no evidence for reorientation of polarity. Instead, statistical analysis shows that cotyledons contain a pre-existing transverse excess in BRXL2 polarity orientation that is not significantly modified by applied tension. The transverse excess reflects BRXL2 being preferentially localized toward the medial side of the cell, nearer to the cotyledon midline, creating a weak medial bias. A second polarity marker, BREAKING OF ASYMMETRY IN THE STOMATAL LINEAGE (BASL), also exhibits weak medial bias in stomatal lineages, whereas ectopic expression of BASL in non-stomatal cells exhibits strong proximal bias, as previously observed in rosette leaves. This proximal bias is also unperturbed by applied tension. Our findings therefore show that cotyledons contain two near-orthogonal coordinated biases in planar polarity: mediolateral and proximodistal.

RESULTS AND DISCUSSION

Stomatal development provides a model system for understanding the control of asymmetric division and patterning in plants.⁹ Several stomatal proteins are localized in a polarized and dynamic manner during stomatal lineage development.^{2,4,10,11} Tissue-wide mechanical forces have been proposed to play a role in controlling this localization pattern.⁸ Following cell ablation, BREVIS RADIX-LIKE 2 (BRXL2) polarity protein becomes oriented toward the ablation site, suggesting that gradients in wall stresses generated by ablation may provide an orienting cue. An alternative explanation is that ablation generates a molecular wound signal that orients BRXL2 toward the ablation site.

More direct evidence for the role of mechanical stresses comes from experiments in which BRXL2 polarity was quantified in cotyledons mechanically stretched transverse to their midline.⁸ Cotyledons were chosen for this experiment because

they show little evidence of tissue-wide polarity for BRXL2, in contrast to rosette leaves which show significant proximal bias (localization at the cell end nearer the leaf base). Cotyledons of live seedlings can also be readily stuck down on stretchable membranes. The previously published results showed that in unstretched controls, BRXL2 polarity exhibited no significant excess in the transverse orientation, whereas in stretched cotyledons, BRXL2 polarity became significantly aligned transversely, parallel to the stretch orientation.⁸ This observation raises the question of how BRXL2 polarity in individual cells changes following stretching.

Sequential imaging reveals no significant stretch-induced change in BRXL2 localization

To answer this question, we developed a rig that allowed the same cotyledons to be imaged before and after stretching (Figure 1A). In addition to the *BRXL2pro:BRXL2-YFP* marker, we

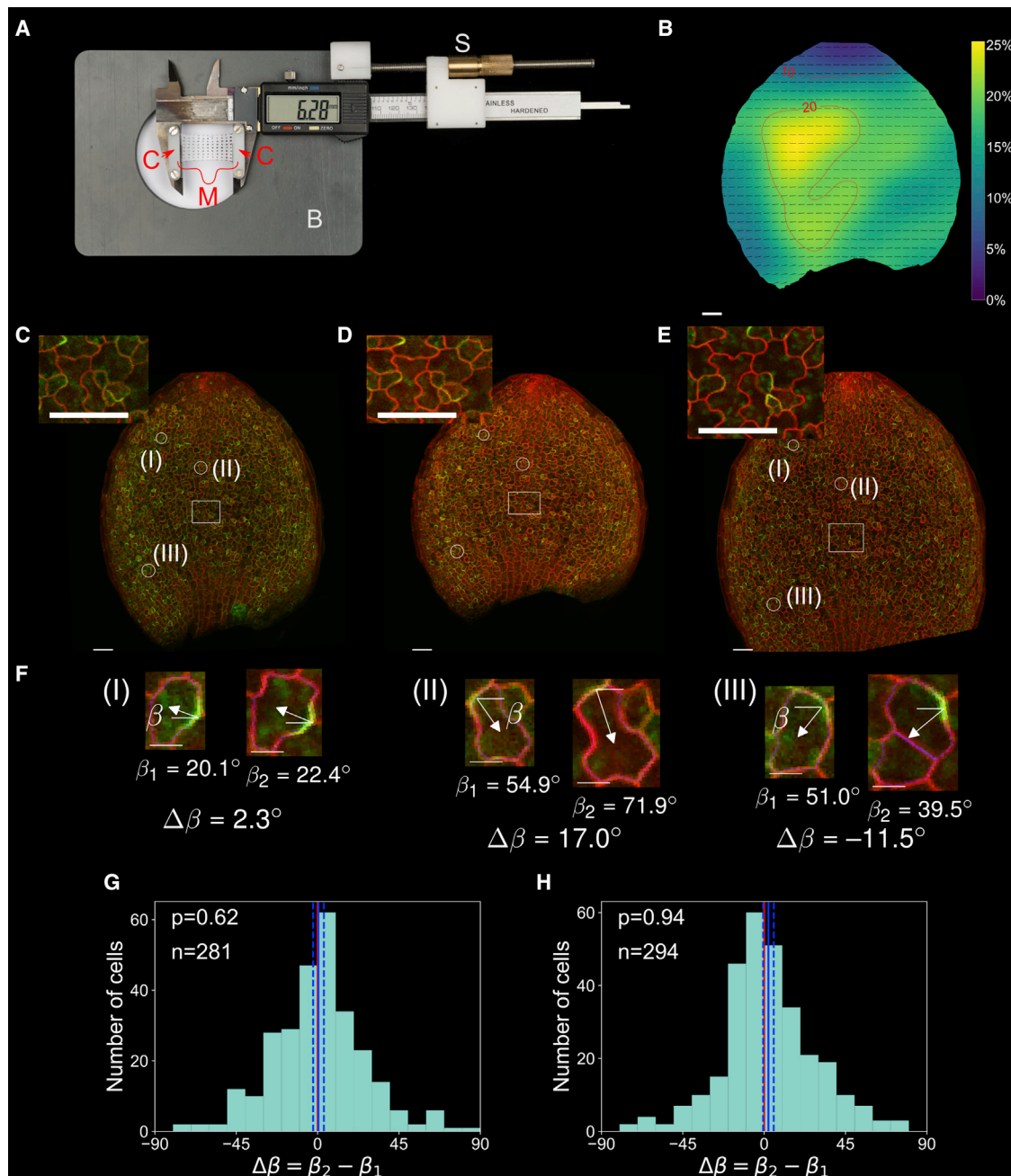


Figure 1. Tracked changes in BRXL2 polarity orientation in response to mechanical stretching

(A) Stretching rig. Cotyledons are glued to an elastic membrane (M), attached to calipers via clasps (C). Degree of stretching controlled by adjustment screw (S), used for opening, closing, and locking the caliper. The caliper is mounted on a base (B) that fits on the microscope stage.

(B) Quantified deformation caused by stretching a cotyledon. Deformation calculated from nonlinear registration of cotyledons before and immediately after stretching. Black lines indicate local directions of maximum deformation. Color scale indicates stretch anisotropy $\xi = x_2y_1/x_1y_2$, where x_1 and x_2 are the lengths of a small region along the direction of maximum deformation before and after stretching respectively, and y_1 and y_2 are the lengths perpendicular to this direction for the same region. Deformation field computed using a cubic B-spline with 8 intervals in each direction, which may not resolve cellular-scale details.

(C) Cotyledon before stretching. Cell outline (red) and BRXL2 (green) signal from projected confocal stacks. Inset shows magnified image of boxed region. Circles labeled (CI), (CII), and (CIII) indicate the cells in (F).

(D) Same cotyledon as (C) immediately after stretching.

(E) Same cotyledon as (C) imaged following 7 h stretching and released from the membrane.

(F) Measurement of the angle β between the BRXL2 polarity vector (from the center of the signal to the cell centroid) and the transverse axis (perpendicular to the cotyledon midline). Left images show the cotyledon before stretching (as in C), right images show the cell after a 7 h stretch followed by release from the membrane (as in E). $\Delta\beta$ was calculated by subtracting β_1 before stretching from β_2 after a 7 h stretch.

(legend continued on next page)

crossed in a mCherry membrane-marker to identify cell outlines. Before stretching (Figure 1C), polarized BRXL2 signal on the abaxial surface could be seen in about 12% of cotyledon cells (1,701/14,535, 13 cotyledons from 9 seedlings 3–4 days old), reflecting the subset of cells undergoing stomatal lineage divisions. We then glued the cotyledons to an elastomer membrane (*m* in Figure 1A), which was stretched by 60% in a direction perpendicular to the cotyledon midline, as previously described.⁸ As in the previous study, a 60% membrane stretch led to a more elliptical shape in the stretch direction (Figure 1D). We calculated the deformation for each region of the cotyledon by nonlinear registration of images before and after stretching¹² and found that the degree of deformation anisotropy varied from over the cotyledon, indicating variable adhesion of the glue (Figure 1B). Previous experiments also described a much lower level of cotyledon deformation compared to the membrane.⁸ Cotyledons were kept in the stretched condition for 7 h, as previously described, and then imaged under a coverslip after release from the stretch (Figure 1E). A decrease in width/length ratio of the cotyledon upon stretch release was checked to ensure that the cotyledon remained under tension for 7 h. We analyzed 13 cotyledons from 9 individuals, before and after 7 h stretching. As controls, we also analyzed 10 cotyledons from 7 individuals that had not been stretched during the 7 h period.

BRXL2 signal exhibits a highly dynamic pattern in stomatal lineages, appearing 5 ± 2.5 h before an asymmetric division and persisting for 9 ± 2.5 h afterward.¹¹ For cells that could be readily tracked, we detected BRXL2 in 14% of cotyledon cells before stretching (1,353/9,784 tracked cells). In 21% (281/1,353) of these cells, signal was still detected in the cell after the 7 h stretch, allowing shifts in BRXL2 polarity to be measured directly (individual cell images provided in Data S1 and S2). To quantify orientation, we drew arrows from the center of BRXL2 signal to the cell centroid (corrected by cell segmentation) (Figure 1F). We then measured the magnitude of the angle β between the BRXL2 polarity vector and the line transverse to the midline (parallel to the stretch orientation). This angle varied from 0° (transverse to the midline) to 90° (parallel to the midline). We measured the value of β before (β_1) and after the stretch (β_2) and calculated the difference $\Delta\beta = \beta_2 - \beta_1$. Polarity reorientation in the direction of stretching should produce a decrease in β (i.e., mean $\Delta\beta$ should be negative). We found $\Delta\beta$ had a unimodal distribution that varied from about -45° to $+45^\circ$, indicating fluctuations in BRXL2 localization and/or arrow positioning (Figure 1G). Mean $\Delta\beta$ was $+0.5^\circ$ (SD 25.3° , $n = 281$; Figure 1G) and not significantly smaller than zero ($p = 0.62$, one-sample one-sided *t* test). Controls that had not been stretched gave a similar distribution of $\Delta\beta$ (Figure 1H). Thus, there was no evidence from direct tracking that BRXL2 polarity shifted to align with the orientation of stretching.

Unstretched cotyledons exhibit transverse excess in BRXL2 localization

Given our inability to detect changes in BRXL2 polarity through direct tracking, we made statistical comparisons between unstretched and stretched cotyledons to check whether our results replicated the previously described stretch-induced changes in polarity.⁸ This previous study analyzed a total of 3,571 cells covering four treatments (i.e., about 900 cells per treatment, if all treatments had a similar sample size). The treatments comprised one unstretched control and three different stretch intensities (20%, 40%, and 60%), with 10 or more individuals per treatment. Measurements were made of the angle α between BRXL2 cell polarity and the midline vector of the cotyledon. Angles were classified as transverse ($|\alpha| = 80^\circ\text{--}100^\circ$, parallel to the stretch orientation) or non-transverse (all other angles). For a uniform distribution, $20/180 = 11.1\%$ of cells should exhibit transverse angles. The previous study showed that unstretched controls and cotyledons stretched by 20% had a mean of about 10%–11% transverse angles, consistent with a random distribution; whereas cotyledons stretched by 40% or 60% had means of 17% or 18%–19% transverse angles, significantly higher than expected from a random distribution.

We first analyzed our unstretched controls. To reduce sampling effects, we analyzed 6,834 cells taken from 68 cotyledons from 61 individuals. Combining all data revealed a peak for $|\alpha|$ of around $80^\circ\text{--}130^\circ$ with a mode at $100^\circ\text{--}110^\circ$ (Figure 2A). In contrast to the previous study, there was a significant excess of transverse orientations in these unstretched controls (13.7% transverse angles, one-sided binomial test $p = 2.4 \times 10^{-11}$). The distributions of $|\alpha|$ varied considerably between cotyledons (Figure 2B), demonstrating the importance of having a large sample to establish overall trends.

We next analyzed BRXL2 polarity in stretched cotyledons (13 cotyledons from 9 individuals; Figures 2C and 2D). The distribution was not significantly different from the unstretched cotyledons (Kolmogorov-Smirnov test, $D = 0.0378$, $p = 0.11$, $m = 6,834$, $n = 1,175$). However, unlike the unstretched cotyledons, the stretched cotyledons showed no significant transverse excess (11.8% transverse angles, $p = 0.23$). To check whether this difference might be caused by the lower number of individuals analyzed in the stretched group (13 cotyledons) compared to the unstretched control (68 cotyledons), we randomly sampled 20 groups of 13 cotyledons from the unstretched controls. This sampling produced sample sizes of 1,023–1,411 cells, similar to the number of cells sampled in the previous study for each treatment. The resulting distributions varied, with 16/20 showing significant transverse excess (Figures 2E, 2F, and S1). Thus, the previously reported differences between stretched and unstretched cotyledons⁸ could have been caused by sampling too few cotyledons.

(G) Histogram of $\Delta\beta$ for cells expressing BRXL2 both at the start and the end of the experiment ($n = 281$ cells from 13 cotyledons from 9 different seedlings). $p = 0.62$ from a one-sided *t* test for the distribution mean being less than zero. Blue line shows mean of the distribution ($\mu = 0.5^\circ$), dotted blue lines 95% confidence intervals of the mean from Student's *t* distribution ($-2.5^\circ < \mu < 3.4^\circ$). Red line at zero.

(H) Histogram of $\Delta\beta$ for cells expressing BRXL2 both at the start and the end of the control (no stretch) experiment ($n = 294$ cells from 10 cotyledons from 7 different seedlings). Blue line shows mean of the distribution ($\mu = 2.3^\circ$), dotted blue lines 95% confidence intervals of the mean from Student's *t* distribution ($-0.6^\circ < \mu < 5.3^\circ$). $p = 0.94$ from a one-sided *t* test for the distribution mean being less than zero.

(B)–(E) and insets: scale bars, 100 μm . (F) Scale bars, 25 μm .

See also Figure S3 and Data S1 and S2.

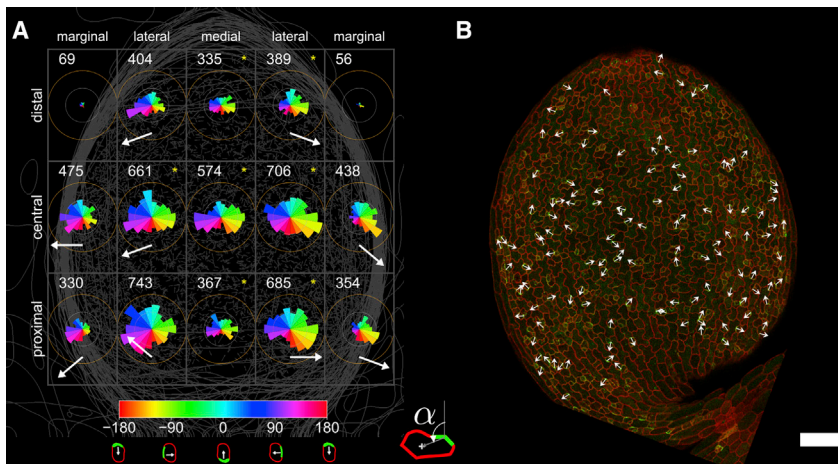


Figure 3. Spatial distributions of BRXL2 and BASL polarity in unstretched cotyledons

(A) BRXL2 polarity pattern. Rose histograms showing the distribution of α for all BRXL2 polarity vectors with an origin that lies within the grid rectangle. Cotyledons manually registered through a combination of translation, scaling, and rotation. Numbers of polarity vectors within each grid rectangle indicated at top. Data omitted from grid rectangles with less than 50 polarity vectors. Arrows show midpoint of modal histogram bins in grid rectangles for which there is a significant excess (two-sided binomial test) of polarity vectors pointing left ($\alpha \geq 0^\circ$) or right ($\alpha < 0^\circ$). Yellow asterisks denote significant ($p < 0.05$) excess of polarity vectors in the transverse range ($80^\circ \leq |\alpha| < 100^\circ$), using one-sided binomial tests. Data from 68 cotyledons from 61 different seedlings. Largest circle = 65 cells.

(B) BRXL2 polarity vectors for a single cotyledon. Cell outlines (red) and BRXL2 (green) signal from projected confocal stack. Vectors adjusted to constant length. Scale bars, 100 μm .

To check for variation caused by sampling cotyledons at different stages, control cotyledons were divided into three groups according to width. All groups had a significant transverse excess (Figure S2). Medium-width cotyledons (550–650 μm) had a significantly different distribution of $|\alpha|$ compared to other groups, though this variation may reflect the small sample sizes per group (19–25 cotyledons per group).

Transverse excess in BRXL2 localization reflects a weak medial bias in stomatal lineages

To investigate the basis of the transverse excess in control cotyledons, we plotted the distribution of α separately for the left and right halves of the cotyledons. Positive values of α indicated polarity vectors pointing leftward and negative value polarity vectors pointing rightward. Left cotyledon halves had an α peak at about $+110^\circ$ whereas right halves had a peak at about -100° and differences between left and right were highly significant (Figure 2G; $p = 2.2 \times 10^{-39}$, chi-squared for cells with positive versus negative α). Thus, transversely oriented BRXL2 polarities tend to point

divergently from the midline, reflecting medial bias of BRXL2 localization.

To quantify the spatial distribution of polarity, we translated, rotated, and scaled control cotyledons to a common template. We then superimposed a rectangular grid of 15 regions over the registered cotyledons and plotted the distributions of α within each region using rose histograms (Figure 3A). For grid regions that showed significant difference between negative and positive α ($p < 0.05$), we plotted the modal orientation of polarity (within the half of the distribution with excess polarity vectors) with a white arrow, and we also indicated those grid regions that showed significant transverse excess with a yellow asterisk. This analysis showed that polarity diverged from the midline, particularly in marginal and lateral positions (Figure 3A). Most of the white arrows pointed slightly downward, as expected from the peak of the distributions in Figure 2G, which were at about 100° rather than 90° . The mediolateral polarity pattern was not evident from inspection of single cotyledons (Figure 3B), indicating medial bias is weak and can only be detected through analysis of many samples. Thus, unstretched cotyledons exhibit a coarse-grain mediolateral polarity field.

so is the midline vector. Data from 68 unstretched cotyledons from 61 different seedlings. Red bar along the x axis indicates the range 80° – 100° of transverse angles used for the significance tests. $p = 2.40 \times 10^{-11}$ from a one-sided binomial test indicates an excess of the proportion of angles within the transverse range (r) over that expected by chance (11%).

(B) Stacked heatmaps of $|\alpha|$ for each cotyledon, in order of increasing cotyledon width (number on left-hand side, in microns). Red crosses indicate the modal histogram bin for each cotyledon.

(C) Histogram of $|\alpha|$ after stretching for 13 stretched cotyledons from 9 plants (data from these cotyledons before stretching is included in A and B). $p = 2.29 \times 10^{-1}$ from a one-sided binomial test as in (A).

(D) Stacked heatmaps for stretched cotyledons.

(E and F) Two different random samples of 13 cotyledons from the dataset in (A), with (E) ($p = 6.85 \times 10^{-9}$) and without (F) ($p = 2.06 \times 10^{-1}$) a significant transverse excess.

(G) Histograms of α with the left (L, blue) and right (R, yellow) cotyledon halves plotted separately. Data from the same 68 cotyledons as in (A). $p = 2.17 \times 10^{-39}$ from a chi-squared test comparing the proportion of cells with positive versus negative α in the left and right halves.

(H) Histograms of $|\alpha|$ for native BASL. Data from 17 unstretched cotyledons. $p = 4.85 \times 10^{-5}$ from a one-sided binomial test as in (A).

(I) Stacked heatmaps of $|\alpha|$ for native BASL.

(J) Histograms of $|\alpha|$ for ectopic BASL. Data from 8 unstretched cotyledons from 7 plants. $p = 1.00$ from a one-sided binomial test as in (A).

(K and L) Histograms as in (G), for native and ectopic BASL, respectively. $p = 8.63 \times 10^{-5}$ (K) and $p = 6.31 \times 10^{-6}$ (L) from chi-squared tests as in (G).

Comparison brackets show the results of two-sample K-S tests between histograms: (A–C) $D = 0.0378$, $p = 0.11$, $m = 6,834$, $n = 1,175$; (A–H) $D = 0.138$, $p = 8.8 \times 10^{-23}$, $m = 6,834$, $n = 1,663$; (C–H) $D = 0.170$, $p = 7.8 \times 10^{-18}$, $m = 1,175$, $n = 1,663$. n.s. indicates $p > 0.05$, **** $p < 0.0001$.

See also Figures S1 and S2.

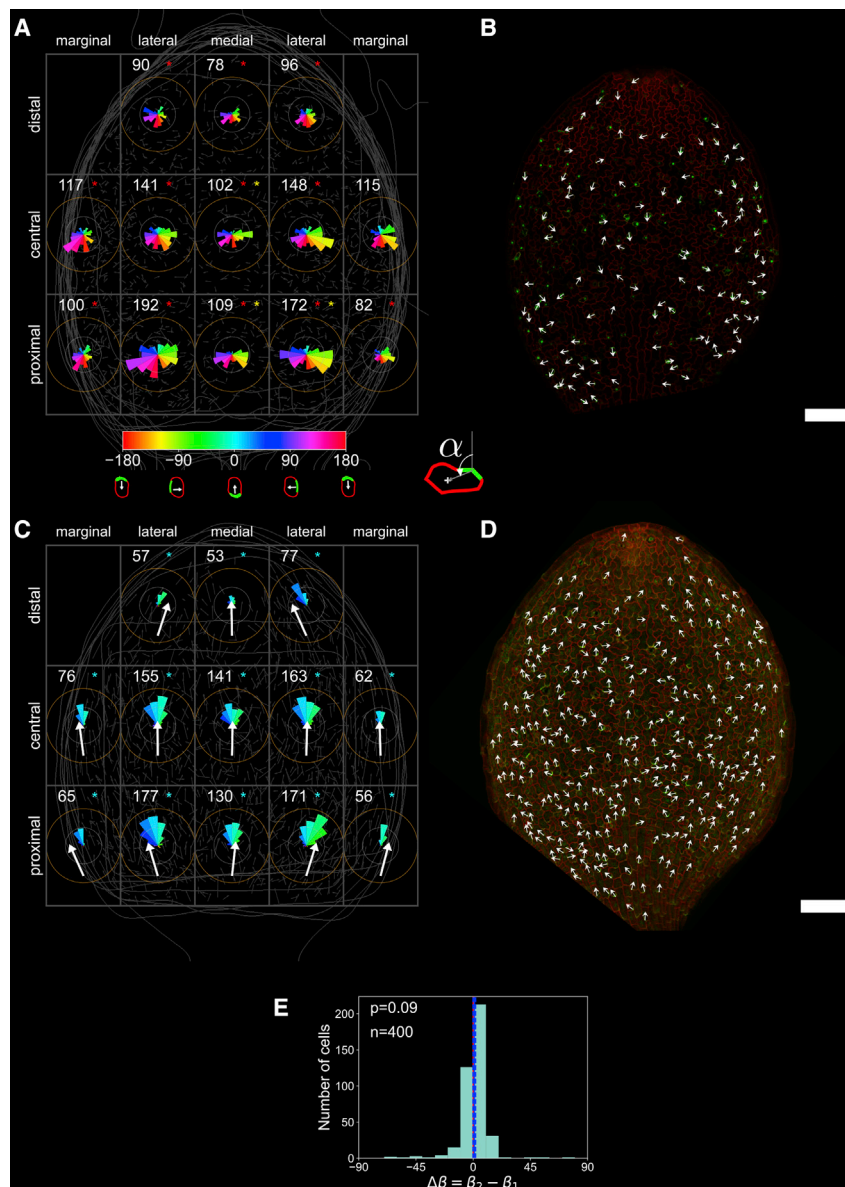


Figure 4. Spatial distributions of BASL polarity in unstretched cotyledons

(A) Endogenous BASL polarity pattern. Rose histograms showing the distribution of α for polarity vectors with an origin that lies within the grid rectangle. Numbers of polarity vectors within each grid rectangle indicated at top. Data omitted from grid rectangles with less than 50 polarity vectors. Red asterisks denote significant ($p < 0.05$) excess of polarity vectors pointing proximally ($|\alpha| > 90^\circ$) compared with distally ($|\alpha| \leq 90^\circ$), using two-sided binomial tests. Yellow asterisks denote significant ($p < 0.05$) excess of polarity vectors in the transverse range ($80^\circ \leq |\alpha| < 100^\circ$), using one-sided binomial tests. Data from 17 cotyledons from 17 seedlings. Largest circle = 25 cells.

(B) Endogenous BASL polarity vectors in a single cotyledon. Cell outlines (red) and BASL (green) signal from projected confocal stack. Vectors adjusted to constant length. Scale bars, 100 μm .

(C) Ectopic BASL polarity. Cyan asterisks denote significant ($p < 0.05$) excess of polarity vectors pointing distally ($|\alpha| \leq 90^\circ$) compared with proximally ($|\alpha| > 90^\circ$), using two-sided binomial tests. Yellow asterisks denote significant ($p < 0.05$) excess of polarity vectors in the transverse range ($80^\circ \leq |\alpha| < 100^\circ$), using one-sided binomial tests. White arrows show (circular) mean polarity direction. Data from 8 cotyledons from 7 seedlings. Largest circle = 45 cells. Data omitted from grid rectangles with less than 50 polarity vectors.

(D) Ectopic BASL polarity in a single cotyledon. Cell outlines (red) and BASL (green) signal from projected confocal stack. Vectors adjusted to constant length. Scale bars, 100 μm .

(E) Histogram of $\Delta\beta$ for cells expressing ectopic BASL both at the start and the end of stretching experiment. $p = 0.09$ from a two-sided t test for the distribution mean being different to zero. Blue line shows mean of the distribution ($\mu = 0.90^\circ$), dotted blue lines 95% confidence intervals of the mean from Student's t distribution ($-0.15^\circ < \mu < 1.94^\circ$). Red line at zero.

Polarity bias in cotyledons varies between stomatal and non-stomatal lineages

BRXL2 colocalizes with another stomatal polarity protein, BREAKING OF ASYMMETRY IN THE STOMATAL LINEAGE (BASL).¹¹ To determine whether BASL polarity also exhibits mediolateral bias in stomatal lineages of cotyledons, we imaged the distribution of *BASLpro::BASL-GFP* in 17 unstretched cotyledons from 17 different plants. The distribution of $|\alpha|$ showed a transverse excess but was significantly different to the BRXL2 distribution (compare Figure 2H to Figure 2A). Relative to BRXL2, there was a deficit of low values of $|\alpha|$, indicative of a slight distal bias, and the peak was shifted slightly from 100° – 110° to about 120° – 140° . The difference between BRXL2 and BASL distributions may reflect the observation that BRXL2 polarizes earlier than BASL and stays polarized for longer.¹¹

As with BRXL2, there was a significant difference in α between left and right cotyledon halves for BASL, indicative of medial bias

(Figure 2K; $p = 8.7 \times 10^{-5}$). The left halves had a peak at about $+130^\circ$ whereas right halves had a peak at about -110° . Grid rose plots indicated that this distribution reflected a coarse-grain mediolateral polarity, though the sample size within each grid was smaller than that used for BRXL2 (Figure 4A). As with BRXL2, mediolateral polarity was not evident from inspection of a single cotyledon (Figure 4B). Thus, in cotyledons both BRXL2 and BASL localization exhibit a weak but significant bias toward medial locations, giving a polarity that points away from the midline.

The medial bias for BRXL2 and BASL in cotyledons contrasts with the situation in rosette leaves where both BRXL2 and BASL exhibit a proximal bias.^{8,13} The proximal bias in rosette leaves is stronger when BASL is expressed outside stomatal lineages.¹³ To determine the polarity pattern for ectopic BASL in cotyledons, we quantified α in 35S:*BASL-GFP*. Polarity was mainly derived from non-stomatal cells, both because these were in excess

and because the promoter used (CaMV 35S) typically gave weak signal in stomatal lineage cells. The distribution of $|\alpha|$ peaked near 0° , suggesting strong proximal bias (Figure 2J). The distribution was almost complementary to that of stomatal BASL (compare Figure 2J with Figure 2H), indicative of orthogonal polarity patterns.

The proximodistal polarity field for ectopic BASL was evident both at the coarse-grain level (Figure 4C) and from inspection of cells from individual cotyledons (Figure 4D), indicating a stronger tissue-wide bias compared to stomatal lineages. Polarity pointed slightly divergently from the midline at the base of the cotyledon, accounting for the slight but significant difference in the α peak between left and right halves of the cotyledon (Figure 2L).

Ectopic BASL persisted in a greater fraction of cells than endogenous BRXL2, allowing the change in orientation, $\Delta\beta$, to be measured for most (400/504) tracked cells initially expressing BASL, after stretching for 7 h. For ectopic BASL, $\Delta\beta$ was not significantly different from 0 (Figure 4E; $p = 0.09$ for one-sample two-sided t test, 95% confidence interval for mean change $-0.15 < \Delta\beta < 1.94$), showing that stretching had no significant effect on ectopic BASL polarity orientation.

Origin of polarity patterns

Cotyledons exhibit two types of bias in BASL/BRXL2 polarity markers: strong proximal bias in non-stomatal lineages and weak medial bias in stomatal lineages. In rosette leaves, both markers exhibit proximal bias, though this is weak in stomatal lineages.^{8,13} One explanation for the weaker bias within stomatal lineages is that two polarizing mechanisms compete in these cell types. Division patterns in primary stomatal lineages depend on a polarity switching mechanism, involving BASL.¹⁰ Polarity switching generates diverse polarity orientations that would tend to disrupt tissue-wide polarity, accounting for the weak biases observed in stomatal lineages. However, it is unclear why the weak bias in stomatal lineages is proximal in leaves and medial in cotyledons. Although the weak biases observed in stomatal lineages may confer little or no selective advantage for stomatal spacing, the underlying polarity systems that generate such biases may play fundamental roles in patterning and orienting other processes, such as growth.

In the case of cotyledons, the coarse-grain mediolateral polarity in stomatal lineages is approximately orthogonal to the polarity in non-stomatal lineages. Orthogonal tissue cell polarity fields have been described for markers such as PIN and SOSEKI proteins,^{3,5} although these are apical-basal versus radial rather than operating within the same epidermal plane. Orthogonal planar polarity patterns have also been described during development of the *Drosophila* wing, where core PCP polarity proteins reorient to align with the proximodistal axis, while Fat system polarity proteins remain aligned with the anteroposterior (mediolateral) axis.¹⁴

How might the orthogonal polarities observed in cotyledons be coordinated? One hypothesis is that chemical signals provide cues,^{15–18} with one set of molecules propagating between cotyledon base and tip to coordinate proximodistal polarity, and another set between midline and cotyledon margin to coordinate mediolateral polarity. A variant of this hypothesis is that chemical signals establish one polarity field (e.g., proximodistal) and the

second is defined orthogonal to this. However, this mechanism would require a system to ensure that orthogonal polarity is oriented oppositely for the left and right halves of the cotyledon. It is also possible that stress gradients provide cues.⁷ If so, they must be robust to externally applied tissue-wide stresses, as both the mediolateral and proximodistal patterns are unperturbed by stretching. Further studies are needed to determine the underlying cues guiding orthogonal polarities and how they influence polarity coordination.

STAR★METHODS

Detailed methods are provided in the online version of this paper and include the following:

- KEY RESOURCES TABLE
- RESOURCE AVAILABILITY
 - Lead contact
 - Materials availability
 - Data and code availability
- EXPERIMENTAL MODEL AND SUBJECT DETAILS
 - Growth conditions
- METHOD DETAILS
 - Preparation of elastomer membrane
 - Stretching cotyledons
 - Microscopy
 - Image processing
- QUANTIFICATION AND STATISTICAL ANALYSIS
 - Analysis for untracked cells
 - Analysis for cotyledons imaged before and after stretching
 - Analysis of spatial distribution of polarity (Figures 3 and 4)
 - Projection of three dimensional stacks to two dimensional images
 - UNet segmentation of two-dimensional cotyledons
 - Quantification of stretching

SUPPLEMENTAL INFORMATION

Supplemental information can be found online at <https://doi.org/10.1016/j.cub.2022.09.049>.

ACKNOWLEDGMENTS

We would like to thank Martyn Hewett for help design and modify the stretching rig, Dominique Bergmann for helpful discussions and providing plant lines, the JIC Bioimaging facility for help with confocal microscopy, and Horticultural services for looking after *Arabidopsis* plants. This research was supported by grants from the UK Biotechnology and Biological Sciences Research Council (BB/W007924/1, BBS/E/J/000PR9787, BBS/E/J/00000152, BB/L008920/1, and BBS/E/J/000PR9789) awarded to E.C.

AUTHOR CONTRIBUTIONS

M.Y., J.A.F., W.B., J.S., C.M., J. Chan, and E.C. conceived and designed the study. M.Y., W.B., J.A.F., J. Cheng, and J.S. acquired data and developed resources. E.C., C.M., and J. Chan provided supervision. J.A.F. and E.C. wrote the manuscript. All authors reviewed and revised the manuscript.

DECLARATION OF INTERESTS

The authors declare no competing interests.

INCLUSION AND DIVERSITY

We support inclusive, diverse, and equitable conduct of research.

Received: May 12, 2021

Revised: June 22, 2022

Accepted: September 26, 2022

Published: October 17, 2022

REFERENCES

1. Truernit, E., Bauby, H., Belcram, K., Barthélémy, J., and Palauqui, J.C. (2012). OCTOPUS, a polarly localised membrane-associated protein, regulates phloem differentiation entry in *Arabidopsis thaliana*. *Development* **139**, 1306–1315.
2. Dong, J., MacAlister, C.A., and Bergmann, D.C. (2009). BASL controls asymmetric cell division in *Arabidopsis*. *Cell* **137**, 1320–1330.
3. Krecek, P., Skupa, P., Libus, J., Naramoto, S., Tejos, R., Friml, J., and Zazimalová, E. (2009). The PIN-formed (PIN) protein family of auxin transporters. *Genome Biol.* **10**, 249.
4. Pillitteri, L.J., Peterson, K.M., Horst, R.J., and Torii, K.U. (2011). Molecular profiling of stomatal meristemoids reveals new component of asymmetric cell division and commonalities among stem cell populations in *Arabidopsis*. *Plant Cell* **23**, 3260–3275.
5. Yoshida, S., van der Schuren, A., van Dop, M., van Galen, L., Saiga, S., Adibi, M., Möller, B., Ten Hove, C.A., Marhavy, P., Smith, R., et al. (2019). A SOSEKI-based coordinate system interprets global polarity cues in *Arabidopsis*. *Nat. Plants* **5**, 160–166.
6. Shimotohno, A., Sotta, N., Sato, T., De Ruvo, M., Marée, A.F., Grieneisen, V.A., and Fujiwara, T. (2015). Mathematical modeling and experimental validation of the spatial distribution of boron in the root of *Arabidopsis thaliana* identify high boron accumulation in the tip and predict a distinct root tip uptake function. *Plant Cell Physiol.* **56**, 620–630.
7. Heisler, M.G., Hamant, O., Krupinski, P., Uyttewaal, M., Ohno, C., Jönsson, H., Traas, J., and Meyerowitz, E.M. (2010). Alignment between PIN1 polarity and microtubule orientation in the shoot apical meristem reveals a tight coupling between morphogenesis and auxin transport. *PLoS Biol.* **8**, e1000516.
8. Bringmann, M., and Bergmann, D.C. (2017). Tissue-wide mechanical forces influence the polarity of stomatal stem cells in *Arabidopsis*. *Curr. Biol.* **27**, 877–883.
9. Bergmann, D.C., and Sack, F.D. (2007). Stomatal development. *Annu. Rev. Plant Biol.* **58**, 163–181.
10. Robinson, S., Barbier de Reuille, P., Chan, J., Bergmann, D., Prusinkiewicz, P., and Coen, E. (2011). Generation of spatial patterns through cell polarity switching. *Science* **333**, 1436–1440.
11. Gong, Y., Varnau, R., Wallner, E.S., Acharya, R., Bergmann, D.C., and Cheung, L.S. (2021). Quantitative and dynamic cell polarity tracking in plant cells. *New Phytol.* **230**, 867–877.
12. Arganda-Carreras, I., Sorzano, C.O.S., Marabini, R., Carazo, J.M., Ortiz-de Solorzano, C., and Kybic, J. (2006). Consistent and elastic registration of histological sections using vector-spline regularization. In *Computer Vision Approaches to Medical Image Analysis (CVAMIA 2006)*, 4241 (Springer), pp. 85–95.
13. Mansfield, C., Newman, J.L., Olsson, T.S.G., Hartley, M., Chan, J., and Coen, E. (2018). Ectopic BASL reveals tissue cell polarity throughout leaf development in *Arabidopsis thaliana*. *Curr. Biol.* **28**, 2638–2646.e4.
14. Merkel, M., Sagner, A., Gruber, F.S., Etournay, R., Blasse, C., Myers, E., Eaton, S., and Jülicher, F. (2014). The balance of prickle/spiny-legs isoforms controls the amount of coupling between core and fat PCP systems. *Curr. Biol.* **24**, 2111–2123.
15. Abley, K., De Reuille, P.B., Strutt, D., Bangham, A., Prusinkiewicz, P., Marée, A.F., Grieneisen, V.A., and Coen, E. (2013). An intracellular partitioning-based framework for tissue cell polarity in plants and animals. *Development* **140**, 2061–2074.
16. Bayer, E.M., Smith, R.S., Mandel, T., Nakayama, N., Sauer, M., Prusinkiewicz, P., and Kuhlemeier, C. (2009). Integration of transport-based models for phyllotaxis and midvein formation. *Genes Dev.* **23**, 373–384.
17. Smith, R.S., Guyomarc'h, S., Mandel, T., Reinhardt, D., Kuhlemeier, C., and Prusinkiewicz, P. (2006). A plausible model of phyllotaxis. *Proc. Natl. Acad. Sci. USA* **103**, 1301–1306.
18. Chan, J., Mansfield, C., Clouet, F., Dorussen, D., and Coen, E. (2020). Intrinsic cell polarity coupled to growth axis formation in tobacco BY-2 cells. *Curr. Biol.* **30**, 4999–5006.e3.
19. Nelson, B.K., Cai, X., and Nebenführ, A. (2007). A multicolored set of in vivo organelle markers for co-localization studies in *Arabidopsis* and other plants. *Plant J.* **51**, 1126–1136.
20. Abramoff, M.D., Magalhaes, P.J., and Ram, S.J. (2004). Image processing with ImageJ. *Biophotonics Int.* **11**, 36–42.
21. Schindelin, J., Arganda-Carreras, I., Frise, E., Kaynig, V., Longair, M., Pietzsch, T., et al. (2012). Fiji: an open-source platform for biological-image analysis. *Nat. Methods* **9**, 676–682. <https://doi.org/10.1038/nmeth.2019>.
22. Rueden, C.T., Schindelin, J., Hiner, M.C., DeZonia, B.E., Walter, A.E., Arena, E.T., et al. (2017). ImageJ2: ImageJ for the next generation of scientific image data. *BMC Bioinformatics* **18**, 529. <https://doi.org/10.1186/s12859-017-1934-z>.
23. Seabold, S., and Perktold, J. (2010). Statsmodels: econometric and statistical modeling with python. In *Proceedings of the 9th Python in Science Conference*, p. 92.
24. Virtanen, P., Gommers, R., Oliphant, T.E., Haberland, M., Reddy, T., Cournapeau, D., Burovski, E., Peterson, P., Weckesser, W., Bright, J., et al. (2020). SciPy 1.0: fundamental algorithms for scientific computing in Python. *Nat. Methods* **17**, 261–272.
25. R Core Team (2016). *A Language and Environment for Statistical Computing* (R Foundation for Statistical Computing). <http://www.R-project.org/>.
26. Weigert, M., Schmidt, U., Boothe, T., Müller, A., Dibrov, A., Jain, A., Wilhelm, B., Schmidt, D., Broaddus, C., Culley, S., et al. (2018). Content-aware image restoration: pushing the limits of fluorescence microscopy. *Nat. Methods* **15**, 1090–1097.
27. Ronneberger, O., Fischer, P., and Brox, T. (2015). U-net: convolutional networks for biomedical image segmentation. In *International Conference on Medical Image Computing and Computer-Assisted Intervention (Springer)*, pp. 234–241.
28. Sitzmann, V., Martel, J.N.P., Bergman, A.W., Lindell, D.B., and Wetzstein, G. (2020). Implicit neural representations with periodic activation functions. In *Conference on Neural Information Processing Systems (NeurIPS 2020)*, pp. 1–12.

STAR★METHODS

KEY RESOURCES TABLE

REAGENT or RESOURCE	SOURCE	IDENTIFIER
Chemicals, peptides, and recombinant proteins		
SYLGARD 182 Silicone Elastomer kit (0.5 kg)	Ellsworth Adhesives	Cat#4019601
Medical Adhesive	Adapt 7730	Cat#7730
Deposited data		
Confocal leaf images	This paper; osf.io	https://doi.org/10.17605/osf.io/ufzj5
Experimental models: Organisms/strains		
Arabidopsis plants containing BRXL2::BRXL2-YFP	Bringmann and Bergmann ⁸	N/A
Arabidopsis plants containing 35S::GFP-BASL	Dong et al. ²	N/A
Arabidopsis plants containing BASL::GFP-BASL and mCherry-plasma membrane		
Arabidopsis plants containing PM-mCherry	Nelson et al. ¹⁹	N/A
Arabidopsis plants containing BRXL2::BRXL2-YFP and RFP-mCherry	This paper	N/A
Arabidopsis plants containing 35S::GFP-BASL and PM-mCherry	This paper	N/A
Software and algorithms		
ImageJ	Abramoff et al. ²⁰	https://imagej.nih.gov/ij/
BUnwarpJ	Arganda-Carreras et al. ¹²	https://imagej.net/BUnwarpJ
Custom Python scripts	This paper; Github	https://github.com/jfozard/cotyledon-polarity ; https://doi.org/10.5281/zenodo.7025217

RESOURCE AVAILABILITY

Lead contact

Further information and requests for plant lines, constructs and raw data should be directed to and will be fulfilled by the lead contact, Enrico Coen (enrico.coen@jic.ac.uk).

Materials availability

This study did not generate new unique reagents.

Data and code availability

- Microscopy data reported in this paper have been deposited in osf.io and are publicly available as of the date of publication. DOIs are listed in the [key resources table](#).
- All original code has been deposited at Zenodo and is publicly available as of the date of publication. DOIs are listed in the [key resources table](#).
- Any additional information required to reanalyze the data reported in this paper is available from the lead contact on request.

EXPERIMENTAL MODEL AND SUBJECT DETAILS

Experiments were performed using *Arabidopsis thaliana* (Col-0 background) plants expressing *BRXL2pro:BRXL2-YFP*⁸ or *35Spro:GFP-BASL*² crossed with plants expressing PM-mCherry (PM-rb¹⁹). F2 And F3 seedlings were used for experiments. The *Arabidopsis* plants containing *BASLpro:GFP-BASL* together with mCherry marking the plasma membrane, and those containing *35Spro:GFP-BASL*, were from Dong et al.²

Growth conditions

Plants were grown on plates containing 1 % (w/v) Agar, 0.43 % (w/v) Murashige & Skoog powdered medium including vitamins, 3 mM MES, PH 5.7. Seeds were stratified at 4 °C for 2 days and then germinated in a growth room set at 20 °C. The growth room was

bespoke, fitted with a refrigeration unit from Watford Refrigeration and Air Conditioning LTD. Plates were placed on shelves lit by 3 tubes (Philips, TLD 36W/865) producing a light intensity of 87 $\mu\text{mol}\cdot\text{m}^{-2}\cdot\text{s}^{-1}$. The room was kept under a 16 h light/8h dark cycle. 3 or 4-day old seedlings were used in experiments.

METHOD DETAILS

Preparation of elastomer membrane

Elastomer membrane was prepared by mixing 45 mL of SYLGARD 182 silicone solutions and 5 ml of SYLGARD 182 Silicone Elastomer Curing agent (Ellsworth Adhesives LTD; 4019601). 10 ml of elastomer solution was poured into square petri dishes and allowed to set for 3 days. The membrane was then cut into 3 cm x 1.8 cm strips using a razor blade.

Stretching cotyledons

Stretch experiments were carried out using a modified calliper. The calliper contained clasps on the jaws for fixing the elastomer strip, and a screw for opening/closing and locking the calliper. The calliper was mounted onto a base that fitted onto the stage of the microscope. A hole in the base allowed light to be transmitted through the specimen.

Seedlings expressing either *BRXL2pro:BRXL2-YFP* and PM-mCherry or *35Spro:GFP-BASL* and PM-mCherry were glued on to the elastomer membrane using medical adhesive (Adapt 7730; 7730). This was done by dabbing a spot of glue onto the centre of an elastomer strip. A seedling was then placed upside-down with the adaxial surfaces of cotyledons touching the glue. The proximal-distal axes of the cotyledons were oriented at 90 degrees relative to the long axis of the elastomer strip. The cotyledons were then gently pushed against the glue using a cotton swab. The glue set after at least 3 min. Damp strips of filter paper were then placed over the hypocotyl/roots to prevent the seedlings from dehydrating. Individuals that were damaged during this process were discarded.

The elastomer membrane with glued seedling was then attached to the modified calliper (see [Figure 1A](#)). The calliper was opened until the membrane became straight. The distance between the tips of the calliper was then measured and the stretch applied by opening the calliper by an appropriate amount to stretch the membrane by 60 % stretch. The jaws were then locked tight. A piece of damp filter paper was placed on the base beneath the calliper and a block of agar (cut from the plate used to grow the seedlings) was placed on top the roots. The calliper was wrapped in cling film or sealed in a large square petri dish with damp filter paper and placed in the growth room over the period of stretch.

For each experiment, 5 images of the cotyledons were used: (1) before stretch (x20 lens), (2) immediately upon stretch (x10 lens), (3) after 7 hours of stretch prior to release (x10 lens), (4) after release of stretch before removal from calliper (x10 lens), (5) after release of 7 hour stretch (x20 lens). First images were taken before seedlings were glued on to membrane strips. Second, third and fourth images were taken by placing the calliper in the microscope. For the final image, seedlings were incubated in a few drops of distilled water for 5 min and, when possible, gently removed from the stretched membrane using forceps. If the cotyledons remained firmly attached, the whole membrane was removed from the calliper for imaging. First and final images were taken using a x20 lens and after mounting seedlings under a cover slip with water. These were used for segmentation and analysis. Other images were taken without coverslips using the x10 lens and were just used to ensure successful stretch and that the stretch held for 7 hours. Note that, for a subset of the data, the second and fourth images were not acquired.

Additional images of cotyledons that had not undergone attachment to membrane strips and stretching, imaged under a cover slip using x20 lens, were used to supply the data used in [Figures 2B–2F](#), [2H](#), and [3](#).

Microscopy

Cotyledons were imaged with a Zeiss 780 exciter confocal laser scanning microscope equipped with EC PLAN-NEOFLUAR x10 (NA of 0.3) and Plan-APOCHROMAT x20 (NA of 0.8) objective lenses or a Leica SP8X confocal laser scanning microscope equipped with a PL APO x20 (NA of 0.75) objective lens. GFP and YFP were excited at 488 nm using an Argon ion laser (Zeiss 780) or a Pulsed White Light Laser (Leica SP8) and the emission collected at 490–530 nm. mCherry was excited at 561 nm and the emission collected between 590–640 nm. Confocal sections were collected at a z-spacing of 1–4 μm for x20 images and 5–15 μm for x10 images, with sufficient z depth to capture the width of the cotyledons for subsequent measurement.

To remove autofluorescence, images collected using the Pulsed White light laser were gated so that the first 0.2 ns of emission were not collected.

GFP and mCherry were collected sequentially using the Zeiss 780 and simultaneously using the Leica SP8X confocal microscope.

Image processing

Initial image processing was performed using the Fiji distribution²¹ of the ImageJ software (<https://imagej.nih.gov/ij/>).²² Details of the custom image analysis pipeline used are detailed below. Figure panels were combined using Inkscape.

QUANTIFICATION AND STATISTICAL ANALYSIS

Confocal images of cotyledons were processed using a custom pipeline, described below. Two different procedures were used – one where cells were not tracked before and after stretching, used to generate the data for the histograms in [Figure 2](#), and the spatial data

shown in [Figures 3 and 4](#) (excluding [Figure 4E](#)), and a more complex one where cells were tracked before and after stretching (used to generate the histograms of the change in angle β in [Figures 1G, 1H, and 4E](#)).

Analysis for untracked cells

- (a) Using the stack projection method described below, three-dimensional confocal image stacks ([Figure S3A](#)) were projected to two-dimensional images ([Figure S3B](#)).
- (b) A UNet (a convolutional neural network, described below) was used to predict cell boundaries from the projected wall channel images ([Figure S3C](#)). These boundary predictions were segmented using a watershed method ([Figure S3D](#)), labelling the regions occupied by each cell.
- (c) Using ImageJ, manual line segment annotations ("arrows") were added to those cells in which the marker was clearly polarized. These arrows were drawn starting at the centre of the region occupied by the marker and ending within the polarized cell ([Figure S3E](#)). Multiple arrows were added to each image using the ROIManager and saved as an ImageJ ROI file.
- (d) For each image, the angle θ between the midline vector (proximo-distal axis) of the cotyledon and the positive x-axis was determined by drawing a line in ImageJ along the cotyledon midline, and measuring the angle of this line using the "measure" tool. ([Figure S3F](#)).
- (e) Centroids of segmented cells were calculated, and the end of each arrow was adjusted to be at the centroid of the enclosing cell ([Figure S3G](#)). Angles a between the positive x-axis and the adjusted arrow directions (anti-clockwise angles being positive, and clockwise negative) were calculated. Adjusted arrows where the distance between the original and the adjusted end was more than 1.5 times the original length of the arrow, or where the start point was more than 5 pixels from the cell boundary were discarded, as they are likely associated with segmentation errors.
- (f) Angles α for each arrow, were calculated by subtracting the midline angle θ from a , and remapping the result to the range $-180^\circ < \alpha \leq 180^\circ$.
- (g) To assess whether there was an excess of polarity arrows in the mediolateral directions, one-sided binomial tests were performed, comparing the observed number of arrows for which $80^\circ \leq |\alpha| < 100^\circ$ with $20/180 = 11.1\%$ of the total number of arrows (the proportion that would be expected if the arrows had a uniform random distribution on 0° to 180°), using the alternative hypothesis that there are more arrows in the mediolateral directions. These binomial tests were performed using the python "statsmodels" package function "binom test."²³
- (h) This binomial test was also performed on the aggregated data from 68 unstretched cotyledons ([Figure 2A](#)) 13 stretched cotyledons ([Figure 2C](#)), 17 unstretched cotyledons expressing native BASL ([Figure 2H](#)) and 8 cotyledons expressing ectopic BASL ([Figure 2J](#)). The 68 control cotyledons were shuffled randomly, and tests applied to 20 groups of 13 cotyledons ([Figures 2E, 2F, and S1](#)).
- (i) A two-sample Kolmogorov-Smirnoff test was used to compare the distribution of the angle $|\alpha|$ for the stretched and unstretched cotyledons ("ks_2samp" from Python "scipy.stats"²⁴).
- (j) To explore whether the pattern of marker polarity differed between the left and right-hand sides of the cotyledons, the positions of the cotyledon centers were estimated (through manual alignment with a template, [Figure S3H](#)). This allowed the arrows to be divided according to whether their base lay on the left of right hand side of the cotyledon. Separate histograms of α were calculated for the polarity arrows in each of these two regions.

Analysis for cotyledons imaged before and after stretching

- (a) Three dimensional stacks were projected to two-dimensional images as before.
- (b) The UNet described below was used to predict cell boundaries. For one of the stretched ectopic BASL cotyledons, segmentations were further refined through the removal of small cells and manual merging and splitting of cells, as the automatic segmentation was not acceptable for this cotyledon
- (c) Again, manual line segment annotations indicating marker polarization were added.
- (d) The angle θ between the midline vector and the x-axis was measured for each image (before and after stretching).
- (e) Centroids of segmented cells were calculated, and the end of each arrow was adjusted to be at the centroid of the containing cell. For the BASL marker, in a small number of cases, arrows were accidentally added in the opposite direction: if the end of an arrow was further from any cell-cell interface than the start of the arrow, this was corrected by reversing the arrow before adjusting the arrow end.
- (f) Non-rigid registration, using the ImageJ plugin bUnwarpJ¹² was used to find the deformation map between material points before stretching (T1) and immediately after release from the membrane (T3) ([Figure S3Ii](#)).
- (g) This deformation map was used to identify corresponding cells at the two timepoints. More precisely:
 - (i) The segmentation at T3 ([Figure S3Iii](#)) was transformed to the coordinate system of T1 using the deformation map from T1 to T3. (Each pixel was given the label of the corresponding pixel in the segmentation at T3. See [Figure S3Iiii](#)).
 - (ii) Each cell in the deformed T3 segmentation was linked to the cell which it maximally overlapped in the T1 segmentation, provided that this overlap was more than 50% of the area of the cell. This captured all non-dividing and dividing cells.

- (iii) Each cell in the T1 segmentation was linked to the cell which it maximally overlapped in the deformed T3 segmentation, provided this is more than 50% of the area of the cell. This captured events where two cells merge (through under-segmentation at T1).
- (iv) The links from (ii) and (iii) formed a bipartite graph (a graph in which each edge connects members of two different, disjoint sets). The connected components (which we refer to as "tracks") of this bipartite graph were extracted (by breadth-first search on the graph), and classified according to how many cells they contained at T1 and T3.
- (v) Components containing one cell at T1 and one or two cells at T3 were retained, and identified as successfully tracked cells. This was the majority of the dataset. Components not containing one cell at T1 and one or two cells at T3 were discarded.
- (vi) At this point, each track contained one cell at T1, and one or two cells at T3. Each cell was classified according to whether it had a marker arrow (i.e. if one of the marker arrows ends within the segmented region associated with this cell). For those tracks that divide, and where the cell at T1 has a marker arrow, the two daughter cells were ordered such that the cell whose centroid (in the deformed T3 segmentation) was nearest the marker arrow base (before stretching) appeared first. If the cell at T1 had no marker arrow, the two daughter cells were sorted such that the one with the marker arrow appeared first.
- (vii) This allowed each track to be classified as belonging to one of 11 distinct categories, shown in detail in [Figure S3J](#). Each category was labelled by a pair of lists (for T1 and T3), each list element describing if the cells at that timepoint had a marker arrow (1) or not (0).
 - ([1], [1]) - Cell where marker persists without division.
 - ([1], [1,0]) - Cell where marker persists through division cell division.
 - ([1], [1,1]) - Cell where the marker persists through division and new marker appears in the other daughter cell.
 - ([0], [1]) - Cell where marker appears without division.
 - ([0], [1,0]) - Cell where marker appears with division.
 - ([0], [1,1]) - Cell where marker appears in both daughter cells with division.
 - ([1], [0,1]) - Cell where marker is both lost and appears with division.
 - ([1], [0]) - Cell where marker is lost without division.
 - ([1], [0,0]) - Cell where marker is lost with division.
 - ([0], [0]) - Cell which does not divide, and has no marker at either timepoint.
 - ([0], [0,0]) - Cell which divided, where both the parent cell and neither child cell expresses the marker.
- (g) For each tracked cell in which the marker persisted, namely categories ([1], [1]) ([1], [1,0]) and ([1], [1,1]), the (unsigned) angle β between the marker arrow direction and the midline was measured. This was calculated by taking the angle a between the centroid-adjusted arrow and the x-axis, and subtracting $90^\circ - \theta$, where θ is the manually measured angle between the midline of the cotyledon and the positive x-axis. The angle was remapped to be between -180° and 180° , the absolute value taken, and subtracted from 180° if it exceeded 90° , giving β . The value β_1 , before stretching, was subtracted from the value β_2 , after stretching, to calculate the change $\Delta\beta$. For tracks in the categories ([1], [1,0]) or ([1], [1,1]), where the cell underwent division, the arrow end was adjusted to be at the centroid of the region occupied by both of the two daughter cells after stretching.
- (h) To test the hypothesis that β was decreased by stretching, a one-sample one-sided t-test using the R function "t.test"²⁵ was performed, with the alternative hypothesis that the true mean is less than zero (alternative="less"), accessed via the RPy Python bridge. Confidence intervals on the mean value of $\Delta\beta$ were provided by a one-sample two-sided t-test from the same R function. For ectopic BASL, a two-sided t-test was performed, with the alternative hypothesis that the true mean is non-zero, again using "t.test"

Analysis of spatial distribution of polarity (Figures 3 and 4)

- (a) As for the histograms of angles for untracked cells, the stack was projected to a two-dimensional image, the cells were segmented, arrows were manually added to indicate marker polarity, arrow ends were adjusted to be at the centroids of the segmented cells, arrows where the distance between the original and the adjusted end was more than 1.5 times the original length of the arrow, or where the start point was more than 5 pixels from the cell boundary were discarded, and the angles a between the polarity arrows and the positive x-axis were measured.
- (b) Angles α for each arrow, were calculated by subtracting the midline angle θ from a , and remapping the result to the range $-180^\circ < \alpha - \theta \leq 180^\circ$.
- (c) Each cotyledon was manually aligned with a template through rotation, translation and uniform rescaling ([Figure S3H](#)).
- (d) A 3x5 rectangular grid was placed over the region occupied by the cotyledon template. Each arrow was assigned to the rectangular grid element containing the arrow base.
- (e) Histograms of the angle α were generated for each grid element. (Note that this used the manually determined midline angle θ , rather than the rotation angle of the alignment, for consistency with the other histograms in the manuscript.)
- (f) Statistical significance tests were applied to the distribution of arrows within each grid element. For BRXL2, two tests were performed for each grid element. Firstly, whether there was an excess of leftwards ($\alpha > 0^\circ$) or rightwards ($\alpha \leq 0^\circ$) pointing arrows was examined using a two-sided binomial test. Secondly, whether there were more medio-laterally oriented arrows

($-100^\circ < \alpha \leq -80^\circ$ or $80^\circ \leq \alpha < 100^\circ$; the same one-sided binomial test as for the histograms of Figure 2) than would be expected by chance (11.1%) was tested. For BASL, whether there was an excess of arrows pointing towards the apex of the cotyledon ($|\alpha| > 90^\circ$) or towards the base of the cotyledon ($|\alpha| > 90^\circ$) was examined using a two-sided binomial test. Whether there was an excess of leftwards or rightwards pointing arrows in each grid element was also tested with a two-sided binomial test. No correction for multiple comparisons was applied to these tests.

Projection of three dimensional stacks to two dimensional images

A neural network method based on Weigert et al.²⁶ was used to generate two-dimensional projections of three-dimensional image stacks. This convolutional network, applied to the cell-wall channel, generated weights for each voxel of the image stack, predicting the locations containing the most instructive fluorescence data for cell boundary identification. The projected image was generated by applying the softmax operator to the column of voxels at each position in the x-y plane, and using these weights to calculate the weighted sum of the image in the z-direction (applying this to both the wall and marker channels).

Weigert et al.²⁶ trained their projection network to give results close to those generated by other software. As an alternative approach to training the network, a separate (small) U-Net²⁷ was added downstream of the projected cell wall channel, and used to predict boundary pixels from hand-curated segmentation data (made using max-projected images). The loss for the whole network combined dice and binary cross entropy losses for the reconstruction of boundary pixels with a term penalizing the thickness of the region from which pixel intensity data was projected (more precisely, this term penalized the variance of the distribution given by the projection weights at each x-y position).

To handle more difficult images with signal appearing above or below the cotyledon, a two-step process was adopted. The predicted depths from the first model were used to initialize an Implicit Neural Representation with a Periodic Activation function (SIREN²⁸), used to represent how the z-depth of the cotyledon surface varied in the x-y plane. This representation, along with another parameter controlling the thickness of the projected region, was then optimized to maximize the normalized cross-correlation between the projected image and the cell boundaries predicted by applying the UNet (described below) to the max-projected image.

UNet segmentation of two-dimensional cotyledons

Projected stacks were segmented in a two-step approach. First, a UNet²⁷ was used to predict cell boundaries from the projected cell wall channel; this was a deeper network with more parameters than that used to train the projection method. A small Gaussian blur, with a kernel having variance of 1 pixel in each dimension, was applied, followed by a watershed transformation (“MorphologicalWatershed” function from the ITK library), labelling the individual regions occupied by each cell.

Quantification of stretching

Following projection to two-dimensions, non-rigid registration, using the ImageJ plugin bUnwarpJ¹² was used to find the deformation map between material points before (T1), and immediately after (T2), stretching. A custom Python script was used to process the deformation map between the two timepoints. A Gaussian blur (with radius 3 pixels), followed by thresholding at intensity level 10, applied to the projected wall channel, was used to distinguish the area occupied by the cotyledons at T2. At each pixel within these areas, the degree of deformation anisotropy $\xi = x_2 y_1 / x_1 y_2$ was calculated, where x_1 and x_2 are the lengths of a small region along the direction of maximum deformation before and after stretching, respectively, and y_1 and y_2 are the lengths perpendicular to this direction of the same region.

In practice, ξ was calculated using the gradients (G) of the reverse deformation map taking material points at T2 to those at T1. (This is the deformation map used to overlay the image at T1 onto the image at T2.) The eigenvalues (λ_{max} , λ_{min}) and corresponding eigenvectors (e_{max} , e_{min}) of the right Cauchy-Green inverse deformation tensor ($G^T G$) were calculated at each point – the eigenvector e_{min} associated with the smallest eigenvalue (λ_{min}) being the direction of maximum stretch (at T2). These eigenvalues are associated to the lengths of the small region described above through $\lambda_{min} = (x_1/x_2)^2$ and $\lambda_{max} = (y_1/y_2)^2$, so the deformation anisotropy was calculated as $\xi = \sqrt{\lambda_{max}/\lambda_{min}}$.

Current Biology, Volume 32

Supplemental Information

**Localization of stomatal lineage proteins
reveals contrasting planar polarity patterns
in *Arabidopsis* cotyledons**

John A. Fozard, Man Yu, William Bezodis, Jie Cheng, Jamie Spooner, Catherine Mansfield, Jordi Chan, and Enrico Coen

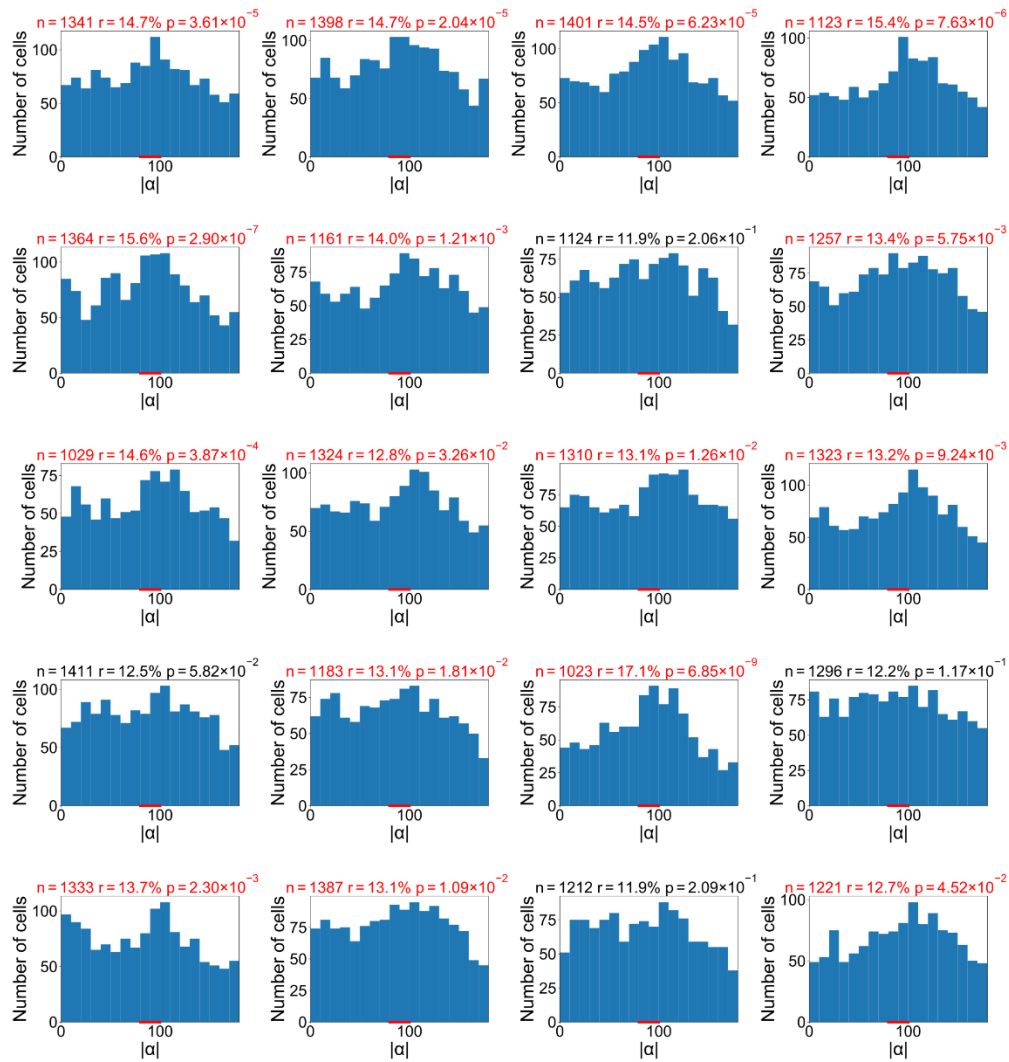


Figure S1. BRXL polarity distributions in samples of unstretched cotyledons, Related to Figure 2. Each histogram shows the distribution of $|\alpha|$, the magnitude of angle between the proximodistal midline vector of the cotyledon and the BRXL2 polarity vector. Each sample contains data from 13 cotyledons, randomly selected from the set of 68 unstretched cotyledons. Red bar along the x-axis indicates the range 80° - 100° of transverse angles used for the significance tests. P-values from one-sided binomial tests, with alternative hypothesis that there is an excess of the proportion of angles within the transverse range (r) than would be expected by chance (11%). Red text indicates samples with statistically significant transverse excess ($p < 0.05$). Note that the data from two of these samples is also presented in Figures 2E and 2F.

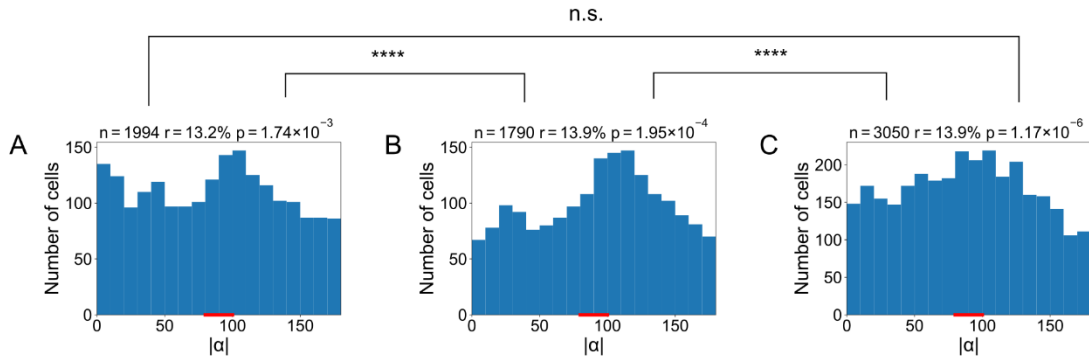


Figure S2. Comparison of BRXL2 polarity distributions for different leaf size classes, Related to Figure 2. Histograms of magnitude of α , the angle between the proximodistal midline vector of the cotyledon and the BRXL2 polarity vector, for unstretched cotyledons with (A) small, $w < 550 \mu\text{m}$ ($n = 24$ cotyledons), (B) medium, $550 \mu\text{m} \leq w < 650 \mu\text{m}$ ($n = 18$ cotyledons), and (C) large $650 \mu\text{m} \leq w$ ($n = 26$ cotyledons), widths w . Red bar along the x-axis indicates the range 80° - 100° of transverse angles used for the significance tests. P-value from one-sided binomial tests indicate an excess of the proportion of angles within the transverse range (r) than expected by chance (11%). Comparisons show results of K-S tests for differences between angle distributions: (A) vs (B) $D=0.073$, $p=8.0 \cdot 10^{-5}$, (A) vs (C) $D=0.035$ $p=0.10$, (B) vs (C) $D=0.084$ $p=2.1 \cdot 10^{-7}$.

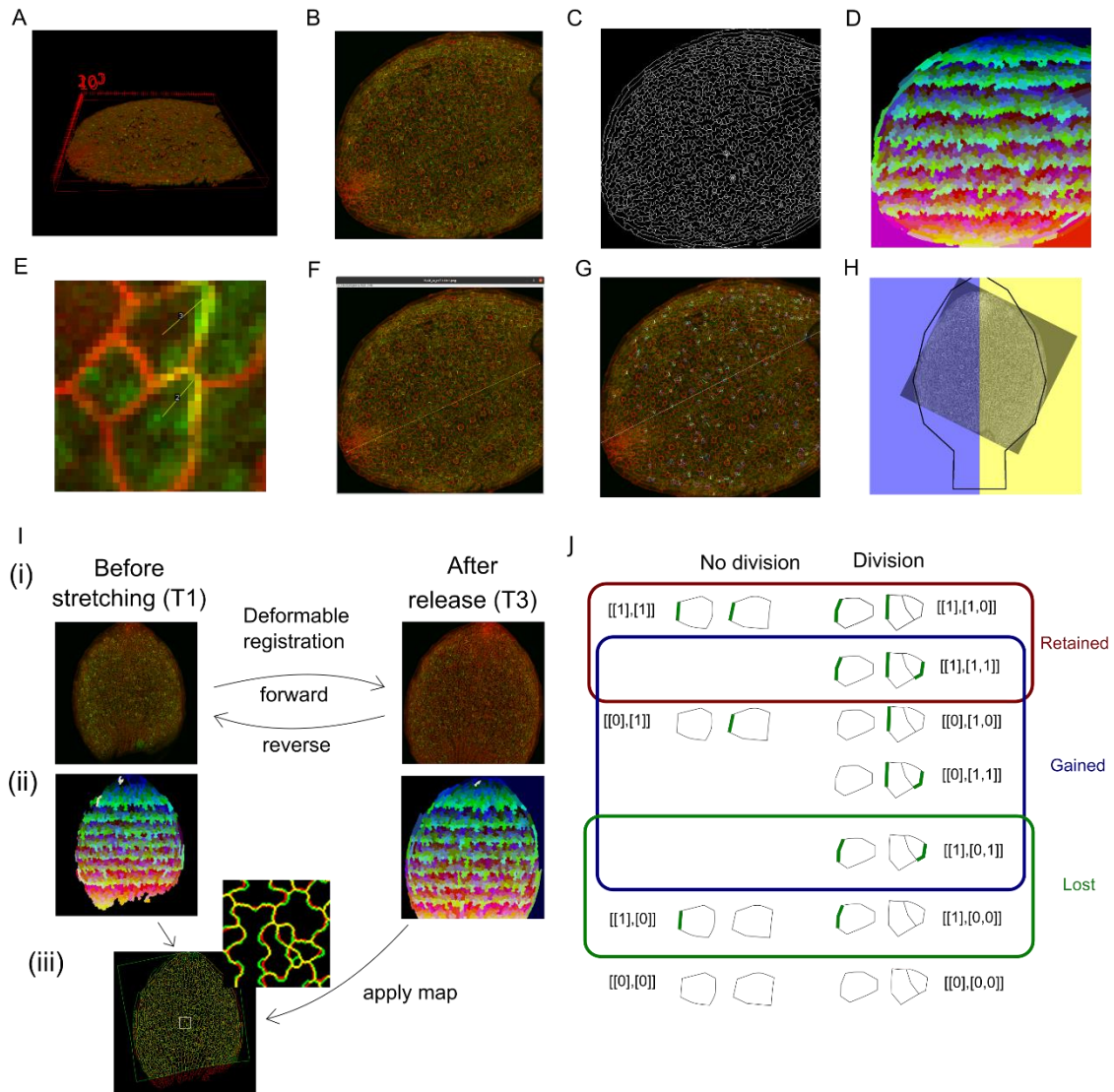


Figure S3 Image analysis pipeline, Related to Figure 1.

(A) Three-dimensional confocal stack of a cotyledon, showing cell membrane (red) and BRXL2 marker (green). **(B)** Two-dimensional projection of stack. **(C)** Detected cell boundaries. **(D)** Watershed segmentation. **(E)** Manual annotation of marker polarities. **(F)** Midline vector direction measurement. **(G)** Polarity arrows adjusted to end at cell centroids, coloured according to angle. **(H)** Manual registration of cotyledon with template. **(I)** Tracking cells between timepoints. (i) Deformable registration used to find forward and inverse maps. (ii) Segmentation before and after stretching. (iii) Overlay of segmentation boundaries before (red) and after (green) stretching at T1, used for cell lineage determination. **(J)** Classification of cell lineages with marker. Green lines indicate presence of marker. Each class is given a unique code (as a pair of lists), denoting the presence or absence of the marker in each cell. List of cells at final timepoint sorted by the distances of cell centroids from marker at initial timepoint (if present).